Supporting Information

Sizable square $CsPb_2Br_5$ nanosheets for photodetection

Shuang Li,[a] Fenyun Wang,[a] Shunhong Dong,[a] Haoyun Dou,[a] Tingfeng Wang [a] and Hong-En Wang*[ab]

[a] College of Physics and Electronic Information, Yunnan Normal University, Kunming 650500, China. E-mail: hongen.wang@ynnu.edu.cn

[b] Yunnan Key Laboratory of Optoelectronic Information Technology, Yunnan Normal University, Kunming 650500, China. E-mail: hongen.wang@outlook.com

Experimental section

Materials

CsBr (purity, 99.5%) and $PbBr_2$ powders (purity, 99.9%) were purchased from Shanghai Macklin Biochemical Co., Ltd. HBr (99.99%) was purchased from Shanghai Aladdin Biochemical Technology Co., Ltd. All the chemicals were used as received without any further purification.

Synthesis of $CsPb_2Br_5$ sheets

The synthesis of the tetragonal $CsPb_2Br_5$ sheets is schematically illustrated in Fig. S1. Initially, 0.04 mmol of CsBr and an equal amount of $PbBr_2$ powders were dissolved in 5 mL of deionized water. The resulting solution underwent heating at 90 °C for 24 h with continuous stirring. Subsequently, 100 μL of HBr solution was introduced to the precursor solution, and the mixture was further heated at 90 °C for an additional 24 h with stirring, yielding the perovskite precursor solution. A 4-inch SiO_2/Si substrate (Zhejiang Lijing Optoelectronics Technology) was cut into 2 cm × 2 cm squares. The SiO_2/Si substrates underwent sequential sonication in acetone, ethanol, and deionized water baths for 15 min each, followed by drying with a nitrogen flow. Finally, the perovskite precursor solution was deposited onto the SiO_2/Si substrate, and the resulting $CsPb_2Br_5$ sheets were obtained after natural drying.

Characterizations

The samples' morphology was examined using a scanning electron microscope (SEM, Quanta FEG 250), and the elemental composition was analyzed through an energy-dispersive X-ray (EDX) analyzer. Atomic force microscopy (AFM) images were acquired on a commercial NX 10 (Park) system. The noncontact mode of AFM was used to investigate the morphology of the samples with a scan rate of 0.4 Hz, a Z Sever Gain of 1.15, and a set point of 15×10^3 nm. The phase structures of the $CsPb_2Br_5$ samples were characterized employing a DX-2700 X-ray diffractometer (XRD). X-ray photoelectron spectroscopy (XPS) analysis of the samples was conducted with a Scientific Escalab 250 XPS spectrometer. Transmission electron microscopy (TEM) and high-resolution TEM (HRTEM) micrographs were captured using a JEM-2100F microscope, operating at 200 kV and equipped with a cold trap. The UV-3600 spectrometer (Shimadzu, Japan) was employed to record the Ultraviolet-visible absorption spectra. Before testing, the instrument's baseline was calibrated with a cuvette containing deionized water. Following calibration, $CsPb_2Br_5$ powder was dispersed in deionized water. The testing procedure utilized an absorption mode within a wavelength range of 300-450 nm, with a step size of 0.5 nm. Steady-state photoluminescence (PL) spectra were acquired using an IK3301 spectrometer with a 325 nm excitation wavelength. Current-voltage (*I-V*) and current-time (*I-t*) curves of the as-fabricated devices were recorded using a semiconductor-integrated test system (Keithley 4200SCS, USA).

Computational details

First-principles density functional theory (DFT) calculations were performed using the Vienna *Ab initio* Simulation Package (VASP) with the Generalized Gradient Approximation (GGA) employing the Perdew-Burke-Ernzerhof (PBE) exchange-correlation functional.[1,2] The projector-augmented wave (PAW) method was utilized to describe the electron-ion interaction. The energy cutoff for the plane-wave basis set was set to 520 eV for $CsPb_2Br_5$ primitive cells. Next, the $CsPb_2Br_5$ (001) surface was cleaved to construct a slab model with a vacuum layer thickness of 12 Å to avoid unwanted mirror interactions. A gamma-centered Monkhorst-Pack scheme was utilized for *k*-point sampling, employing a mesh grid density of 0.04 (2π $Å^{-1}$). Electronic self-consistency was achieved when the energy change between consecutive steps was below 10^{-5} eV/atom, and the forces on each atom converged to less than 0.02 eV/Å. In the surface calculations, dipole corrections along the z-axis and van der Waals interactions were both taken into account using the DFT-D scheme. The adsorption energy (E_{ads}) of a Br or OH on the $CsPb_2Br_5$ (001) surface was computed using the following equation:

$$E_{ads} = E_{(adsorbate\text{-}surface)} - E_{(adsorbate)} - E_{(surface)}.$$

Here, $E_{(adsorbate\text{-}surface)}$, $E_{(adsorbate)}$, and $E_{(surface)}$ denote the total electronic energies of the entire system (a surface adsorbed with one Br or OH), a single Br or OH in vacuum, and the pristine surface, respectively. The calculated data were visualized using VESTA software.[3] Some pre/post treatments for the calculation setup were conducted using the VASPKIT program.[4]

Preparation of the $CsPb_2Br_5$ nanosheets photodetector

The procedure involved securing a SiO_2/Si substrate coated with $CsPb_2Br_5$ nanosheets using a shadow mask, which was wound with a tungsten wire having a diameter of 10 μm. Subsequently, the mask-fixed SiO_2/Si substrate was positioned within the electron beam in the evaporation system, where 80 nm thick Au electrodes were deposited. Following the coating and cooling process, the sample was retrieved, and the two ends of the device, in contact with the Au electrodes, were designated as the selected regions for the photodetector.

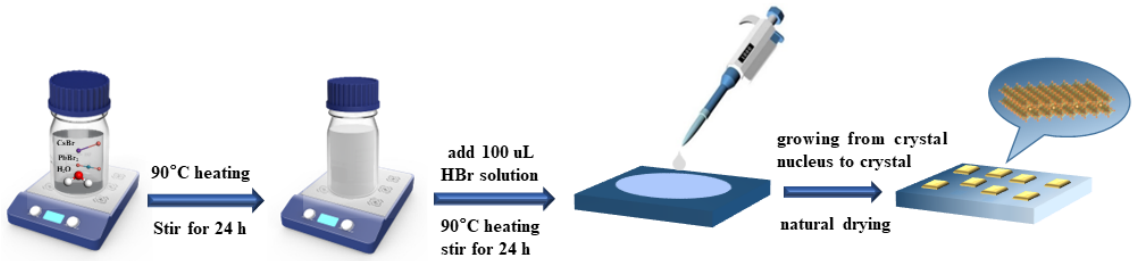

Fig. S1. Schematic synthesis procedure of $CsPb_2Br_5$ nanosheets for photodetector application

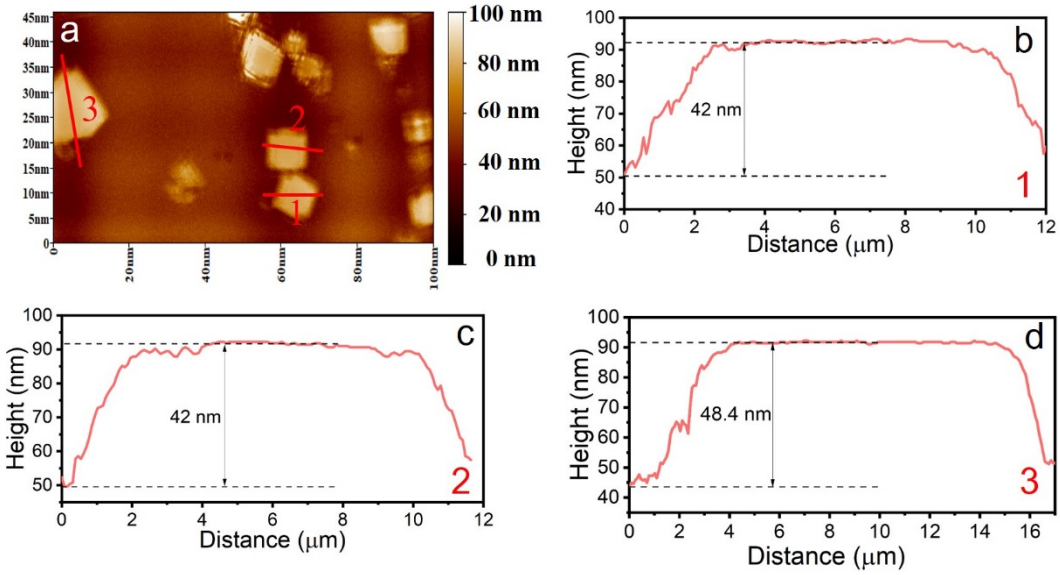

Fig. S2. (a) AFM micrograph and (b-d) corresponding thickness profiles of three $CsPb_2Br_5$ nanosheets, indicating a sheet thickness ranging from 40 to 50 nm

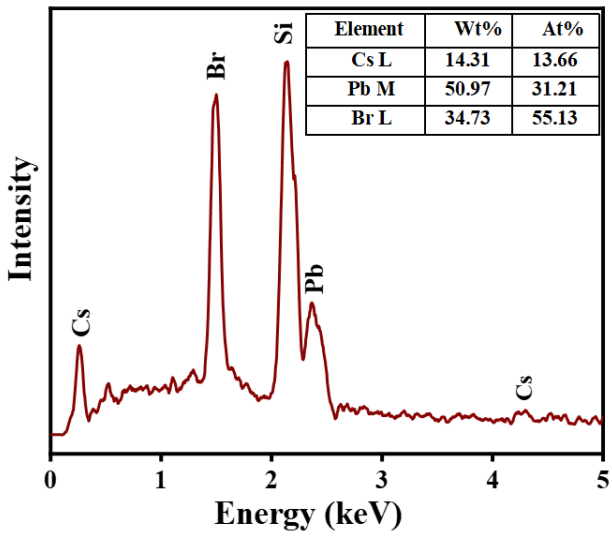

Fig. S3. EDX elemental analysis of $CsPb_2Br_5$ nanosheets

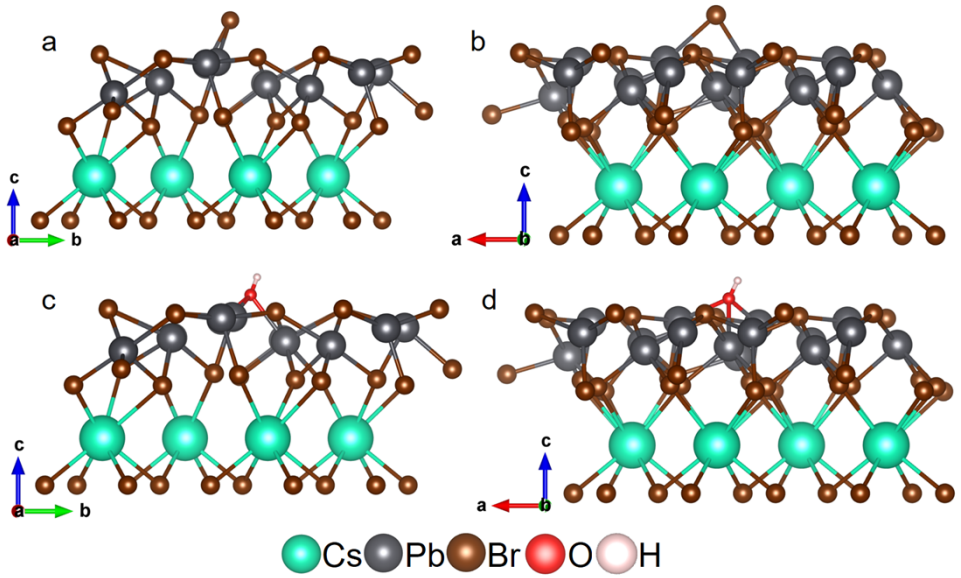

Fig. S4. Optimized geometry configurations of the $CsPb_2Br_5$ (001) crystal facets after adsorption of (a, b) Br, and (c, d) OH molecules, respectively

From **Fig. S4a** and **S4b**, it can be observed that Br tends to adsorb on the $CsPb_2Br_5$ (001) surface, forming a dual coordination with the two exposed Pb atoms on the surface, resulting in an adsorption energy of -2.6 eV. Examining Fig. **S4c** and **S4d**, it is evident that OH exhibits a preference for chemisorption on the surface Pb atoms in a tri-coordinated manner on the $CsPb_2Br_5$ (001) surface, resulting in an adsorption energy of -2.78 eV. The adsorption energy of OH on the $CsPb_2Br_5$ (001) surface is slightly higher than that of Br. However, considering the significantly higher concentration of Br in the solution after the addition of HBr, it is reasonable to infer that the adsorption of Br on the $CsPb_2Br_5$ (001) surface predominates. This suggests that the preferential adsorption of Br on the $CsPb_2Br_5$ (001) surface contributes to the formation of tetragonal $CsPb_2Br_5$ nanosheets.

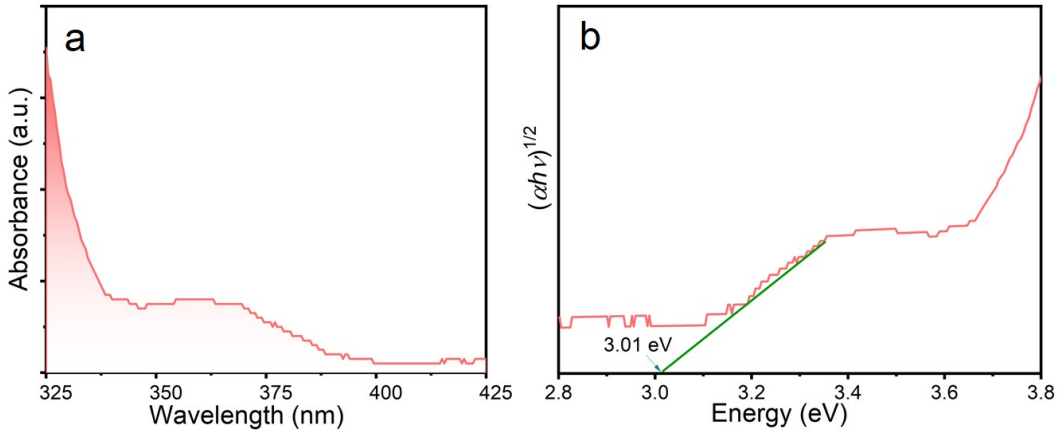

Fig. S5. (a) UV–Vis absorption spectra and (b) the relationship between $(\alpha hv)^{1/2}$ and hv of the $CsPb_2Br_5$ nanosheets

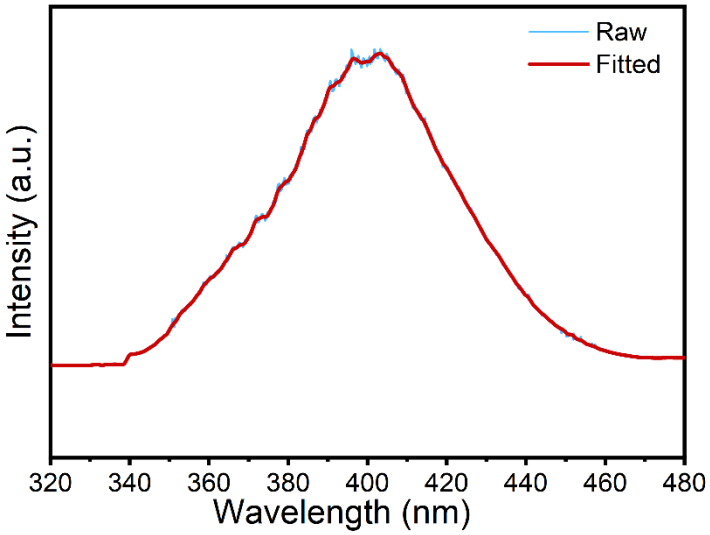

Fig. S6. Photoluminescence (PL) spectra of the $CsPb_2Br_5$ nanosheets

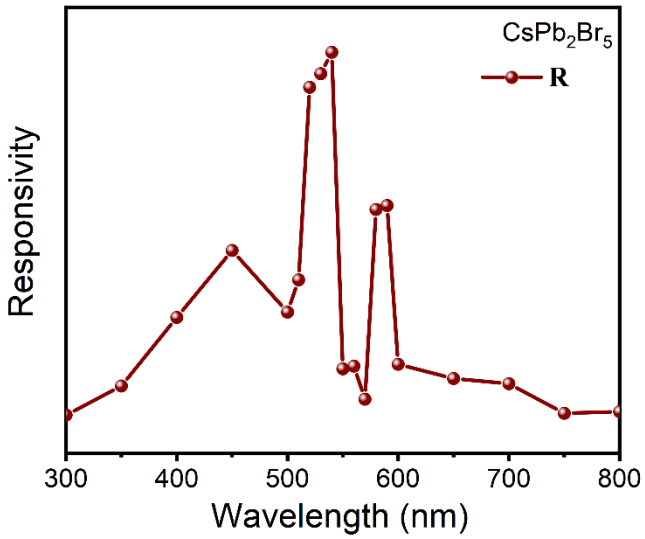

Fig. S7. Spectral responsivity of the $CsPb_2Br_5$ sheets photodetector

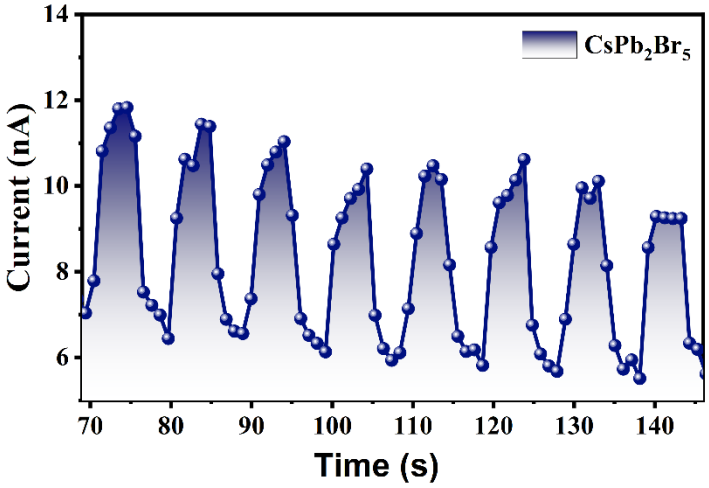

Fig. S8. Relationship between the current and time of a periodically switched light source

Table S1. Optoelectronic Performance comparison of different $CsPb_2Br_5$-based perovskite photodetectors

Material	Method	Wavelength (nm)	I_{light}/I_{dark}	R_λ (A W^{-1})	EQE (%)	D* (Jones)	Rise/decay (ms)	Ref
$CsPb_2Br_5$ NSs	Solution	405	900	0.0754	-	1.33×10^{10}	43/83	5
$CsPb_2Br_5$ NSs	Injection	405	364	0.0004	-	-	426/422	6
$CsPb_2Br_5$ NSs	Injection	405	30	-	-	-	710/600	7
$CsPb_2Br_5$ single crystal	Solution	280	-	0.0251	-	-	40/120	8
2D $CsPb_2Br_5$ phase -$CsPbBr_3$ MW arrays	Two-step	400	1000	7.66	-	4.05×10^{12}	275/550	9
$CsPbBr_3$-$CsPb_2Br_5$ thin films	Vapor	365	13.75	0.375	-	1×10^{11}	0.28/0.64	10
$CsPb_2Br_5$ nanosheets	**Aqueous**	**540**	**2320**	**33.93**	**7716**	**5.98×10^{9}**	**100/180**	**This work**

References

1. J. Perdew, K. Burke and M. Ernzerhof, Generalized Gradient Approximation Made Simple, *Phys. Rev. Lett.*, 1996, **77**, 3865– 3868.

2. G. Kresse and J. Furthmuller, Efficient iterative schemes for ab initio total-energy calculations using a plane-wave basis set, *Phys. Rev. B.*, 1996, **54**, 11169–11186.

3. K. Momma and F. Izumi, VESTA 3 for three-dimensional visualization of crystal, volumetric and morphology data, *J. Appl. Crystallogr.*, 2011, **44**, 1272–1276.

4. V. Wang, N. Xu, J.-C. Liu, G. Tang and W.-T. Geng, VASPKIT: A user-friendly interface facilitating high-throughput computing and analysis using VASP code, *Comput. Phys. Commun.*, 2021, **267**, 108033.

5. R. Wang, Z. Li, S. Li, P. Wang, J. Xiu, G. Wei, H. Liu, N. Jiang, Y. Liu, and M. Zhong, *ACS Appl. Mater. Interfaces*, 2020, **12**, 41919-41931.

6. C. Han, C. Li, Z. Zang, M. Wang, K. Sun, X. Tang, and J. Du, *Photon. Res.*, 2017, **5**, 473-480.

7. X. Tang, S. Han, Z. Zu, W. Hu, D. Zhou, J. Du, Z. Hu, S. Li, Z. Zang, *Front. Phys.*, 2017, **5**, 69.

8. Z. Zhang, Y. Zhu, W. Wang, W. Zheng, R. Lin, F. Huang, *J. Mater. Chem. C*, 2018, **6**, 446-451.

9. G. Tong, M. Jiang, D.-Y. Son, L. K. Ono, Y. Qi, *Adv. Funct. Mater.*, 2020, **30**, 2002526.

10. G. Tong, H. Li, D. Li, Z. Zhu, E. Xu, G. Li, L. Yu, J. Xu, Y. Jiang, *Small*, 2018, **14**, 1702523.